Journal of Applied Physics

RESEARCH ARTICLE | MAY 09 2024

Inerter-controlled topological interface states in locally resonant lattices with beyond-nearest neighbor coupling

Milan Cajić ; Danilo Karličić; Sondipon Adhikari

J. Appl. Phys. 135, 183104 (2024)
https://doi.org/10.1063/5.0205248

AIP Publishing

Journal of Applied Physics ARTICLE pubs.aip.org/aip/jap

Inerter-controlled topological interface states in locally resonant lattices with beyond-nearest neighbor coupling

Cite as: J. Appl. Phys. **135**, 183104 (2024); doi: 10.1063/5.0205248
Submitted: 25 February 2024 · Accepted: 25 April 2024 ·
Published Online: 9 May 2024

Milan Cajić,[1,a)] Danilo Karličić,[1] and Sondipon Adhikari[2]

AFFILIATIONS

[1]Mathematical Institute of the Serbian Academy of Sciences and Arts, 11000 Belgrade, Serbia
[2]James Watt School of Engineering, The University of Glasgow, Glasgow G12 8QQ, United Kingdom

[a)]**Author to whom correspondence should be addressed:** mcajic@mi.sanu.ac.rs

ABSTRACT

This paper explores the emergence of topological interface states in one-dimensional locally resonant lattices incorporating inerters in both nearest neighbor (NN) and beyond-nearest neighbor (BNN) coupling. The investigation focuses on the unique wave propagation characteristics of these lattices, particularly the presence and behavior of interface states. The non-trivial topological behavior due to broken inversion symmetry within the unit cell of the locally resonant lattice is comprehensively investigated in the presence of inerters in NN and BNN coupling. The emerging interface states in the supercell analysis exhibit specific spatial and frequency localization properties due to inerter-based BNN interactions. Additionally, the study demonstrates the ability of inerter elements with weak inertance to control the frequency of interface states while maintaining the fundamental topological properties of the lattice. The identified topological interface states in lattices with BNN coupling present an opportunity for designing diverse devices, such as waveguides, filters, sensors, and energy harvesting systems. Overall, this research enhances our comprehension of topological phenomena in inerter-based locally resonant lattices with BNN interactions and introduces possibilities for creating robust and versatile devices based on topologically protected edge/interface states.

I. INTRODUCTION

In recent years, the field of topological materials has attracted significant attention due to its potential for robust and controllable wave propagation. Topological interface states, in particular, have emerged as a fascinating phenomenon with promising applications in waveguiding, sensing, and signal manipulation. In this study, we investigate the existence and characteristics of topological interface states in one-dimensional inerter-based locally resonant lattices with beyond-nearest neighbor (BNN) coupling.

Locally resonant lattices have been extensively studied for their ability to exhibit interesting band structures and wave propagation properties. The incorporation of inerters, which are passive mechanical elements with tunable dynamic behavior, adds an additional control parameter to the lattice system. Beyond-nearest neighbor coupling, involving interactions between non-adjacent lattice elements, introduces further complexity and potential for non-trivial wave dynamics.

Previous studies have explored topological phenomena in various lattices, including locally resonant and phononic-type periodic mechanical systems. For instance, Zheng *et al.*[1] demonstrated higher-order topological corner states in a two-dimensional elastic locally resonant metamaterial in a deep sub-wavelength regime. Similarly, Zhang *et al.*[2] investigated multimode topological interface states in a one-dimensional 1D elastic-wave phononic system by using the impedance matching method. To characterize the topological properties of one-dimensional periodic structures, one can utilize topological invariants such as Zak phase and/or winding number to determine the non-trivial nature of the bandgaps[3,4] and calculate the number of existing edge states.[5,6] An important issue arises in the calculation of the Zak phase and winding number in multi-band systems.[7] Quantized topological invariants, band inversion, and topological phase transition phenomena are often demonstrated on the Su–Schrieffer–Heeger (SSH) chain model[8] or mechanical lattices with unit cells having inversion symmetry and

centered inversion axis.[9] As revealed in Ref. 10, breaking the inversion symmetry for the centered inversion axis through long-range hooping can yield a non-quantized Zak phase, which also affects the standard formulas for the calculation of the winding number. Some researchers suggested modified formulas for the calculation of the Zak phase to get a quantized topological invariant.[11] When there is a gauge ambiguity in determining the Zak phase, it has been suggested to decompose it into the intercellular and intracellular parts, which enables one to directly calculate the number of edge states by dividing the intercellular part by π.[12] This method is suitable for resolving the mentioned ambiguities in two-band systems while in multi-band systems numerical, such as Willson loop,[13] or analytical approaches[7] can be used to determine the number of edge states.

Recent investigations have focused on studying wave propagation in periodic structures, particularly metamaterials, wherein the physical responses of the system are shaped not only by nearest-neighbor interactions but also by long-range hoppings.[14] These non-local effects can introduce roton-like dispersion behavior in periodic lattices with beyond-nearest neighbor interactions,[15–19] introducing the local maximums and minimums in dispersion curves within the first Brillouin zone. Apart from the roton-like dispersion, long-range hoppings in one-dimensional topological insulators can affect both bulk topological invariants and edge-states due to the existence of hidden symmetries.[20] Longer-range interactions can yield higher winding/chern numbers and the number of edge states in one-, two- and three-dimensional systems.[21,22] However, another challenge emerges when determining the winding number in periodic chains with non-local hoppings using conventional formulas, i.e., lesser winding numbers, and therefore the edge states, are predicted than they occur in the representative super-cell model. Therefore, in Ref. 23, the authors suggested two ways of calculating the correct number of edge states in such type of lattices, one based on the peaks (valleys) of the Berry connection and the other based on the Jackiw–Rebbi zero modes.

An important issue in the topological mechanical metamaterials field is how to tailor or tune their band structure and topological properties. There are two main approaches to achieve this, the active one based on active components such as the piezoceramics[24,25] and the passive one based on optimization or tuning of geometrical or material parameters of the system.[26,27] Unique wave propagation and topological properties were obtained in a one-dimensional phononic-like periodic lattice through a passive mechanical component named inerter.[28] In recent years, mechanical inerter devices[29] have been widely exploited by both scientific and engineering communities.[30] In Ref. 31, the model of ideal mechanical inerter was exploited to tune dispersion characteristics of non-trivial bandgaps and interface modes without affecting the topological properties of the locally resonant lattices. However, the investigation of topological interface states in one-dimensional inerter-based locally resonant lattices with beyond-nearest neighbor coupling remains relatively unexplored, presenting an intriguing research opportunity.

This study aims to uncover the tremendous capabilities of mechanical inerters in manipulating the band structure and frequencies of interface modes while preserving the main topological features of the basic lattice configuration. The specific case of a lattice with inerter elements in third-nearest neighbor (TNN) coupling will be comprehensively investigated as a unique example not yet explored in the literature. Values of the inertance parameter in BNN interactions that maintain the original topological properties of the lattice will be separately explored to reveal the limitations and control potential of the inerters. As such, the study is structured as follows: Sec. II presents the basic formulation of the problem, along with the mathematical model and an illustration of the one-dimensional lattice with BNN coupling. In Sec. III, we outline the methodology for investigating the non-trivial topology of the lattice based on the topological invariant Zak phase and discovering band transitions in related bandgaps. The invariant winding number is discussed, and the Berry connection difference is proposed to account for changes in the number of topological states in the system. Section IV provides the main numerical results and a parametric study to understand the behavior of the proposed system, comparing unit cell and super-cell band structures. The final Sec. V concludes with the main findings and suggests ideas for future research directions in the field.

II. SYSTEM FORMULATION AND EQUATION OF MOTION

To begin, we will examine an infinite one-dimensional elastic chain comprising a unit cell consisting of two outer masses and corresponding inner sub-masses, which represent the local resonating units (refer to Fig. 1). All masses are interconnected by springs and inerter elements, with the addition of third-nearest neighbor (TNN) interactions. Notably, the chain's outer masses are connected by springs with alternating stiffness. The motion equations governing a unit cell in this system can be expressed as follows:

$$\begin{aligned} 0 = {} & m_a \ddot{u}_{1a}^p + k_1(u_{1a}^p - u_{2a}^p) + k_2(u_{1a}^p - u_{2a}^{p-1}) \\ & + k_b(u_{1a}^p - u_{1b}^p) + k_c(2u_{1a}^p - u_{2a}^{p+1} - u_{2a}^{p-2}) \\ & + j_b(\ddot{u}_{1a}^p - \ddot{u}_{1b}^p) + j_a(2\ddot{u}_{1a}^p - \ddot{u}_{2a}^{p-1} - \ddot{u}_{2a}^p) \\ & + j_c(2\ddot{u}_{1a}^p - \ddot{u}_{2a}^{p+1} - \ddot{u}_{2a}^{p-2}), \end{aligned} \tag{1}$$

$$\begin{aligned} 0 = {} & m_a \ddot{u}_{2a}^p + k_2(u_{2a}^p - u_{1a}^p) + k_1(u_{2a}^p - u_{1a}^{p+1}) \\ & + k_b(u_{2a}^p - u_{2b}^p) + k_c(2u_{2a}^p - u_{1a}^{p+2} - u_{1a}^{p-1}) \\ & + j_b(\ddot{u}_{2a}^p - \ddot{u}_{2b}^p) + j_a(2\ddot{u}_{2a}^p - \ddot{u}_{1a}^{p+1} - \ddot{u}_{1a}^p) \\ & + j_c(2\ddot{u}_{2a}^p - \ddot{u}_{1a}^{p+2} - \ddot{u}_{1a}^{p-1}), \end{aligned} \tag{2}$$

$$0 = m_b \ddot{u}_{1b}^p + k_b\left(u_{1b}^p - u_{1a}^p\right) + j_b\left(\ddot{u}_{1b}^p - \ddot{u}_{1a}^p\right), \tag{3}$$

$$0 = m_b \ddot{u}_{2b}^p + k_b\left(u_{2b}^p - u_{2a}^p\right) + j_b\left(\ddot{u}_{2b}^p - \ddot{u}_{2a}^p\right), \tag{4}$$

where u_{ja} and u_{jb} for $j = 1, 2$ denotes displacements of outer and inner masses, k_1, k_2 are stiffness of springs connecting outer masses along with inerter element of inertance j_a, k_b and j_b are stiffness and inertance parameters, respectively, of the locally resonant sub-units and k_c and j_c are stiffness and inertance parameters

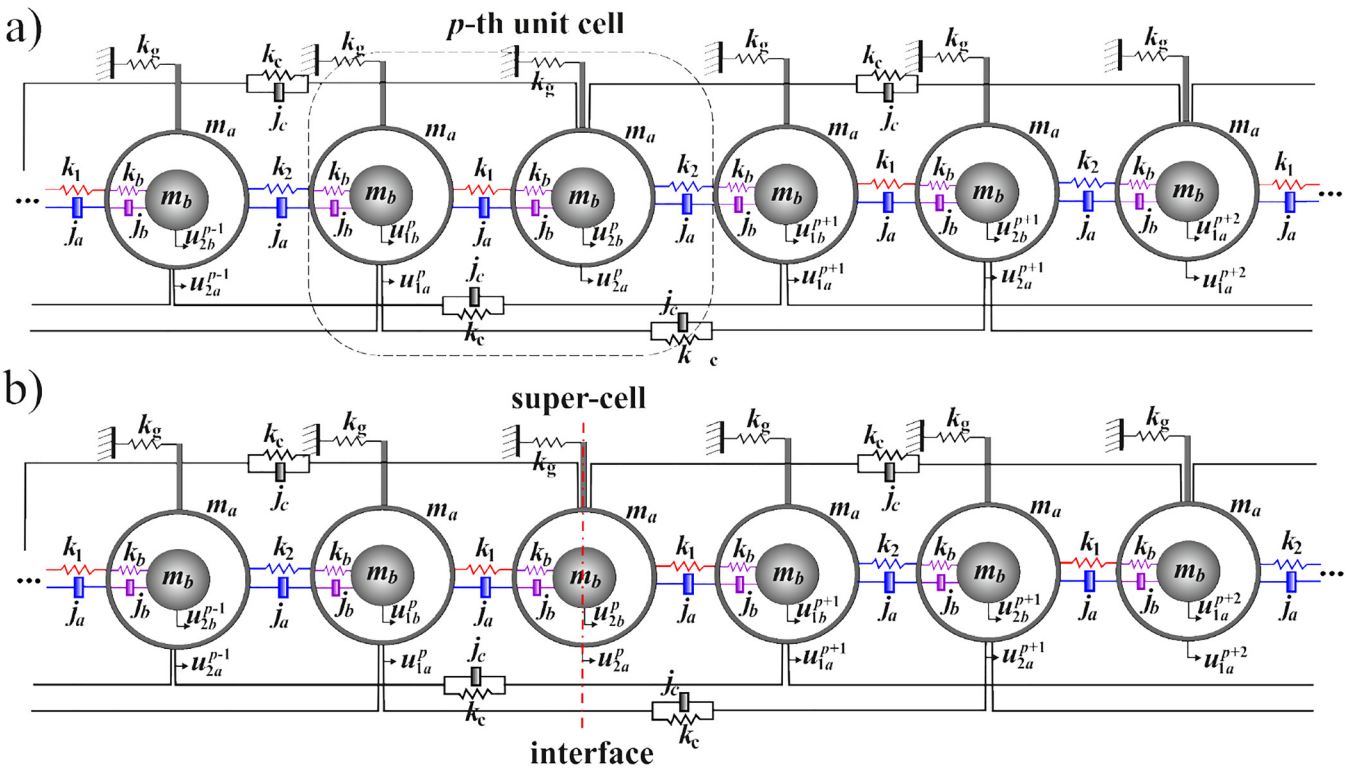

FIG. 1. Illustration of a locally resonant one-dimensional lattice with inerters and TNN couplings (a) representative unit cell; (b) lattice super-cell model with the interface.

representing the TNN interactions. Further, we assume the plane wave solution for the equations of the representative unit cell along with the Floquet–Bloch periodic boundary conditions

$$\mathbf{u}^p = \mathbf{U}(\kappa)\, e^{i(p\kappa d-\omega t)}, \tag{5}$$

where $\mathbf{u}^p = [u_{1a}^p, u_{1b}^p, u_{2a}^p, u_{2b}^p]$ is the vector of displacements of pth unit cell, ω is the frequency, κ is the wavenumber, d is the lattice constant, and $\mathbf{U}(\kappa)$ is the vector of complex wave amplitudes. Substituting this assumed solution into the corresponding equations for the unit cell yields the following eigenvalue problem:

$$\left[\mathbf{K}^p(\kappa) - \omega^2 \mathbf{M}^p(\kappa)\right]\mathbf{U}(\kappa) = 0, \tag{6}$$

where $\mathbf{K}^p(\kappa)$ and $\mathbf{M}^p(\kappa)$ are the corresponding stiffness and mass matrices of the representative unit cell of the periodic 1D chain-like lattice system with TNN couplings. Note that, unlike the classical mass-spring chains, the lattice with inerter elements with both NN and BNN couplings possesses out-of-diagonal elements in the mass matrix, which should be considered when obtaining the dispersion relations and topological invariants.[31] In the following analysis, we will assume the lattice constant as $d = 1$ and solve the above eigenvalue problem to evaluate the dispersion and topological properties of the corresponding lattice system.

III. METHODOLOGY

Solving the above eigenvalue problem equation (6) gives the band structure in terms of the wavenumber for the periodic locally resonant unit cell system having four bands. However, to determine the topological features of eigenvectors associated with these bands, one can utilize the topological invariant Zak phase as a special case of the Berry phase suitable for one-dimensional lattices, that for the mth band is given as

$$\theta_{(m)}^{\mathrm{Zak}} = \mathrm{i}\int_{-\pi}^{\pi} \left[\mathbf{U}_{\mathrm{m}}^{\mathrm{H}}(\kappa)\cdot\partial_\kappa \mathbf{U}_{\mathrm{m}}(\kappa)\right]\mathrm{d}\kappa, \tag{7}$$

where $\mathbf{U}_m^H(\kappa)$ is the Hermitian of the eigenvector $\mathbf{U}_m(\kappa)$. The individual components of eigenvectors $\mathbf{U}_m$ are given as $U_m^{(\alpha)}$ with $\alpha = 1, 2, 3, 4$. In the case of the larger unit cells, with multiple degrees of freedom (more than two), it is more convenient to use the numerical formula for the Zak phase,[3] where a certain number of discretization steps N is used, which is given as

$$\theta_{(m)}^{\mathrm{Zak}} = -\mathrm{Im}\sum_{\mathrm{s}=-\mathrm{N}}^{\mathrm{N}-1} \ln\left[\mathbf{U}_{\mathrm{m}}^{\mathrm{H}}\left(\frac{\mathrm{s}}{\mathrm{N}}\pi\right)\cdot\mathbf{U}_{\mathrm{m}}\left(\frac{\mathrm{s}+1}{\mathrm{N}}\pi\right)\right]. \tag{8}$$

Quantized Zak phase can take the values of 0 or π, which is also connected to the topological invariant winding number $w = \theta_{(m)}^{\mathrm{Zak}}/\pi (\mathrm{mod}\, 2)$ that will take corresponding values of 0 or $w = 1$,

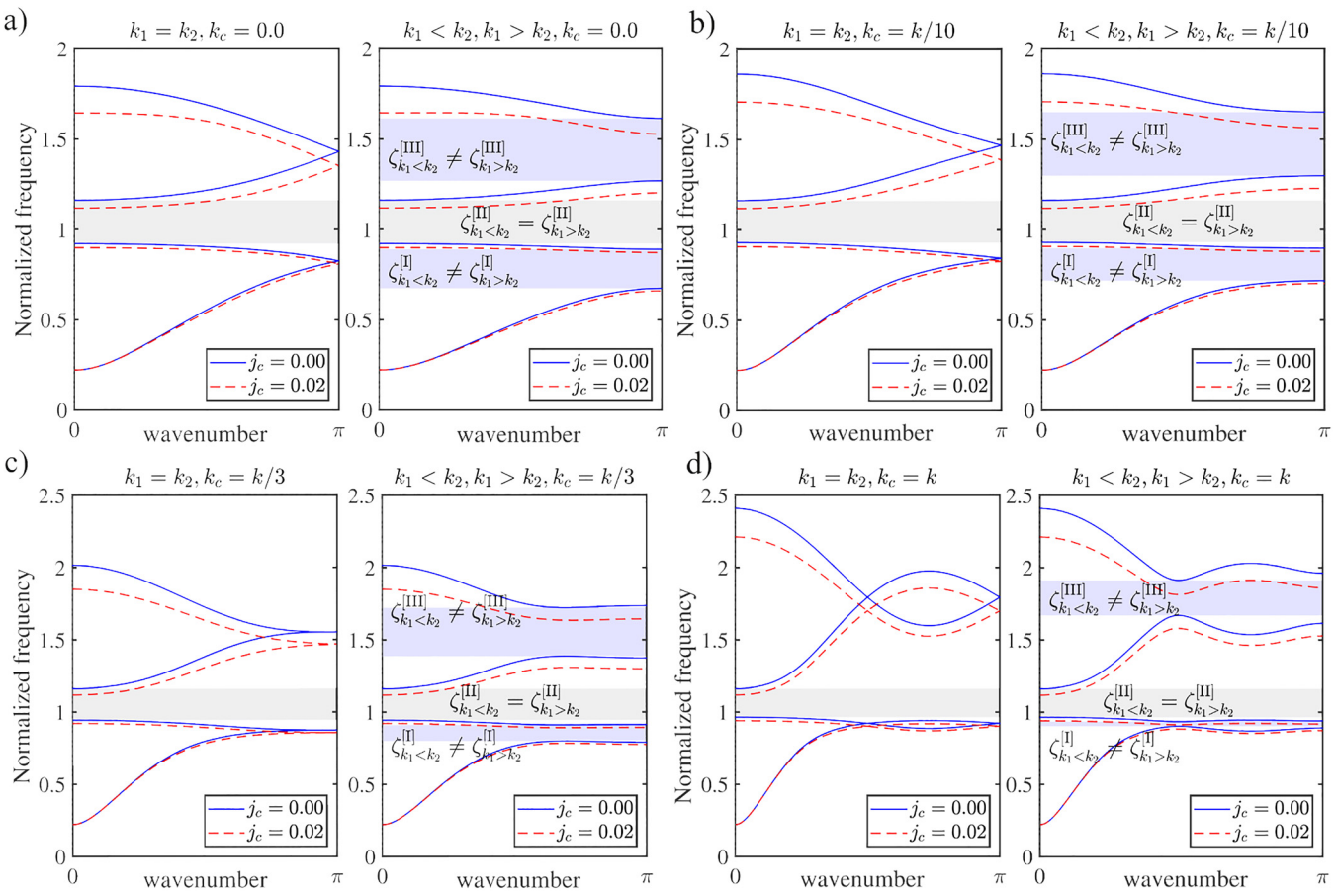

FIG. 2. Band structure diagrams of the inerter-based locally resonant lattice unit cell with TNN coupling through different stiffness springs and inerters. The left side panels in each subfigure show the case when the stiffness band inversion parameter $\gamma = 0$ ($k_1 = k_2$) while the right side panels represent the equal band structures in two configurations $\gamma = \pm 0.5$ ($k_1 \gtrless k_2$). Zak phase of each isolated band is utilized to determine the sign $\zeta^{(n)}$ of the bandgaps and characterize the non-trivial topology of the first and second gap (highlighted in green) and trivial nature of the second gap (highlighted in gray). Red dashed lines show the influence of inerters on band frequencies.

respectively. Additionally, by employing the approach from Ref. 6, the winding number can be visualized through the variation of complex eigenvector components as a function of the wavenumber. This visualization yields three-dimensional plots and rotation of eigenvector components around the center of the complex plane. The first step in this methodology is normalizing eigenvectors to obtain one or more pure real components while the remainder are complex. In simple, two-band systems, this yields one real and one complex component of the eigenvector. A single rotation of the complex component line about the center of the complex plane corresponds to the winding number difference of one. When there are multiple complex components in the normalized eigenvector, the surface connecting these components should also rotate to yield quantized winding number values. In our case, we utilized this procedure to obtain the first two components of eigenvectors as real and the remaining two as complex, which can be further visualized as described above. Moreover, the winding number often corresponds to the number of edge/interface states, giving us precious information about the topological properties of the system. However, when there are BNN interactions, this methodology for counting the number of edge/interface modes in the system breaks down, and other approaches should be used. In Ref. 23, the authors used two approaches, one based on Jackiw–Rebbi (JR) indices associated with JR zero modes, and the second based on the Berry connection curve used to calculate the number of peaks and valleys associated with the number of edge states in the finite lattice. Here, we will employ the conventional numerical formula to calculate the Zak phase of each isolated band to determine the non-trivial nature of certain bandgaps based on the following sign formula:

$$\mathrm{sign}[\zeta^{(n)}] = (-1)^{n}(-1)^{l}\exp\left[\mathrm{i}\sum_{m=1}^{n}\theta^{\mathrm{Zak}}_{(m)}\right], \tag{9}$$

by taking that the first band is $m = 1$, while the first gap $n = 1$ is the

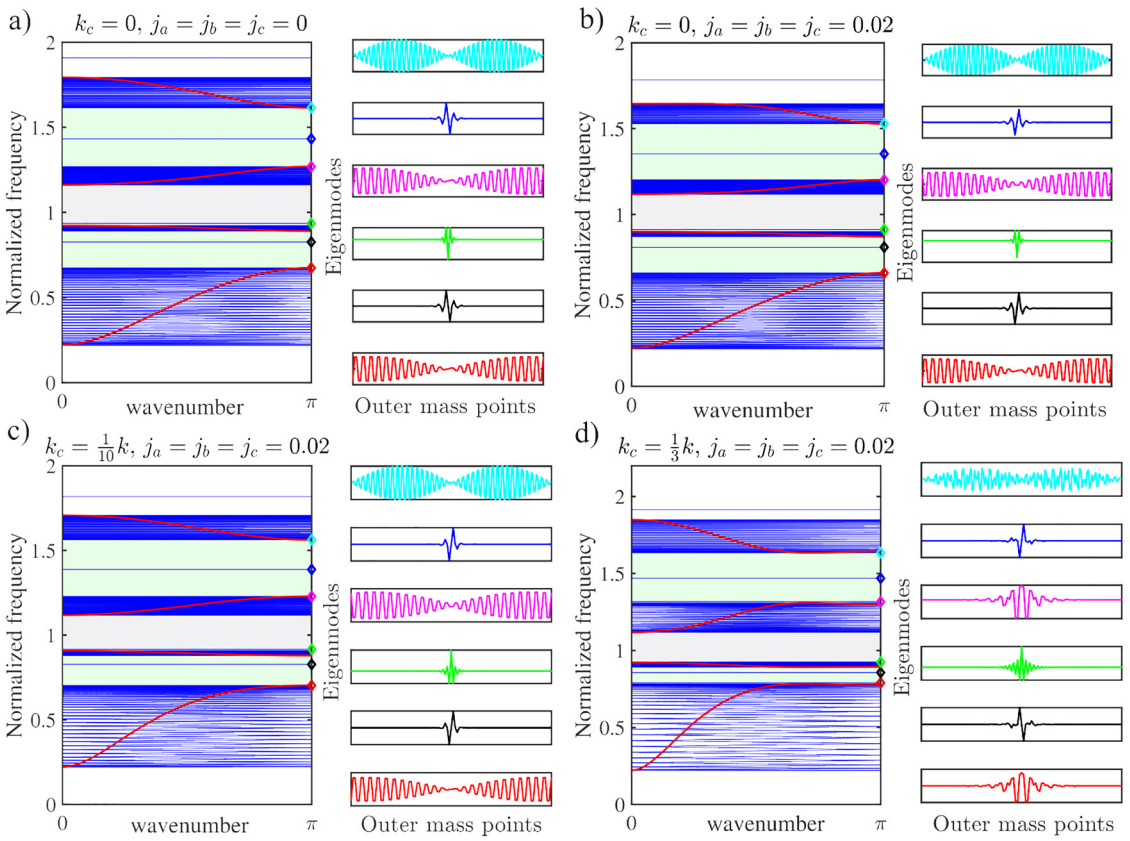

FIG. 3. Band structure and eigenmode diagrams of a supercell with 40 unit cells on each side of the interface (overall 324 masses) without and with low stiffness TNN spring and weak inerter interactions. The case of $\gamma = 0.5$ ($k_1 > k_2$) is adopted in two different configurations: (a) $k_c = 0$ and without inerters; (b) $k_c = 0$ with inerters $j_{a,b,c} = 0.02$; (c) $k_c = 1/10k$ with inerters $j_{a,b,c} = 0.02$; and (d) $k_c = 1/3k$ with inerters $j_{a,b,c} = 0.02$. To distinguish the edge and bulk modes, six chosen frequencies are highlighted in different colors in band structure diagrams (left panels) and corresponding mode shape diagrams (right panels).

one above the first band. By using Eq. (9), one can obtain the corresponding signs of gaps in two lattice configurations and identify nontrivial gaps through opposite signs. However, this information can tell us only about whether the existing edge/interface states will be topologically protected (non-trivial) but does not carry information about their number. For this purpose, similar to Ref. 23, we can calculate the number of TPIS as a topological invariant difference $\Delta B(\kappa) = B_1(\kappa) - B_2(\kappa)$ in the range $\kappa = 0 - 2\pi$, where B_1 and B_2 refers to the cases $k_1 > k_2$ and $k_1 < k_2$, respectively. Here, Berry connection is represented by the integrand of Eq. (7) which can be also obtained numerically similar to Eq. (8). The number of protected states will be confirmed through the super-cell band structure analysis.

IV. RESULTS AND DISCUSSION

This section shows the most important results regarding the band structure, topological, and localization properties of the lattice with the third-nearest neighbor interactions, based on the exploration of a simple unit cell and a super-cell model. This will reveal the main wave propagation behavior of such types of periodic systems and enlighten the potential of inerter elements to manipulate lattice features such as interface mode frequency. The following values of parameters are used in simulations if not given otherwise in figures: stiffnesses $k_1 = k(\gamma + 1)$ and $k_2 = k(\gamma - 1)$ with the mean stiffness $k = 10\,000$ (N/m) and stiffness parameter $\gamma = 0.5$, stiffness of the local resonator $k_b = k/2$, stiffness of the ground spring $k_g = k/10$ and values of outer $m_a = 1$ (kg) and inner $m_b = m_a/3$ masses. The values of inerter parameters, with the same unit of (kg), are given in figures. Note that all the obtained frequencies are normalized with the frequency of the local resonator given as $\Omega_b = \sqrt{k_b/m_b}$.

A. Band structure and topological properties

Let us study the band structure and topological invariants of the unit cell by using Eqs. (1)–(9) that generates dispersion curves and corresponding topological invariant Zak phase for each of the four bands. Figure 2 shows the band structure for different stiffness k_c of springs in the TNN coupling with and without inerters. Moreover, the signs of bandgaps, calculated based on the Zak

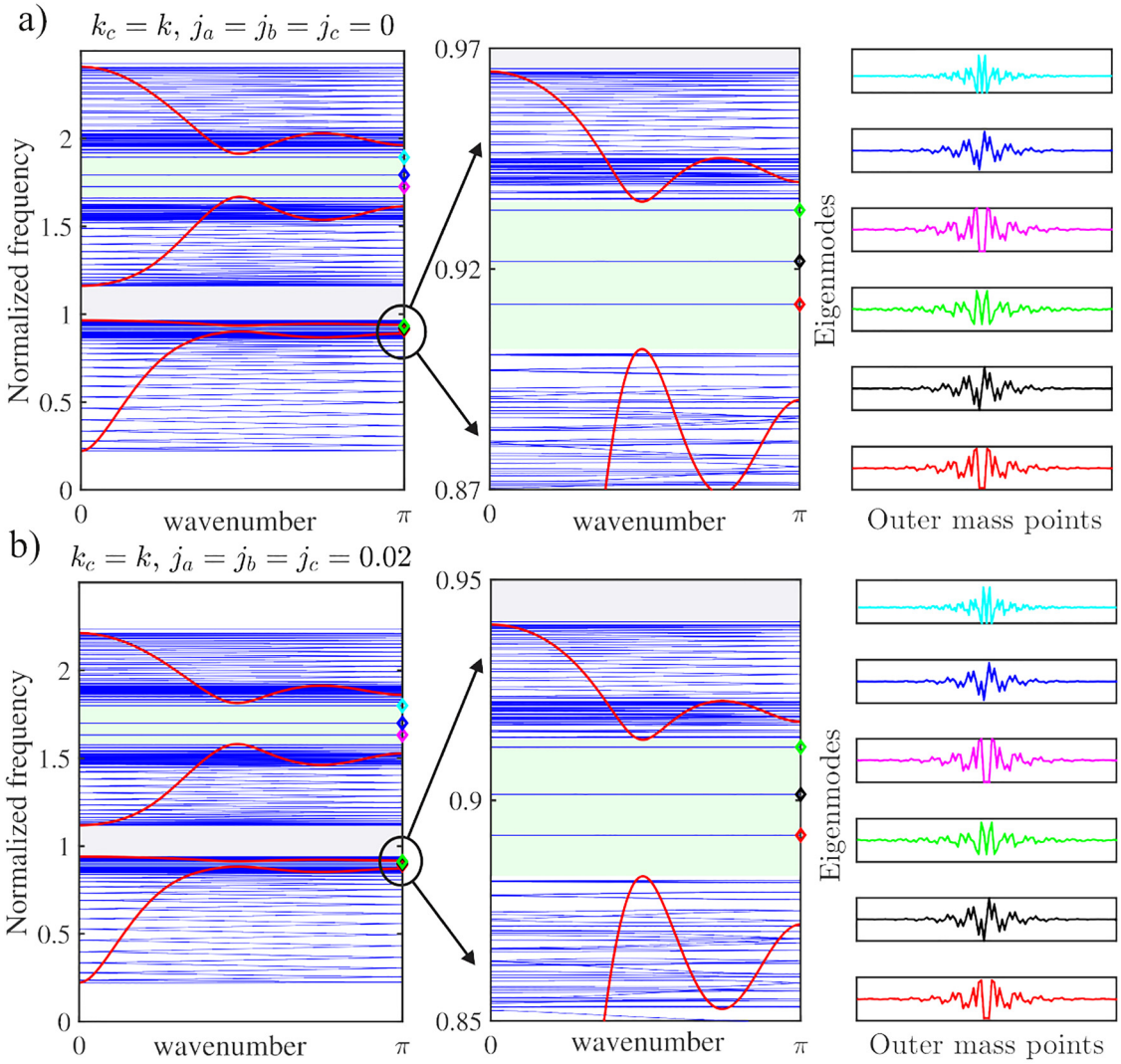

FIG. 4. Band structure and eigenmode diagrams of a supercell with 40 unit cells on each side of the interface (overall 324 masses) with high stiffness TNN spring and weak inerter interactions. The case of $\gamma = 0.5$ ($k_1 > k_2$) is adopted in two different configurations: (a) $k_c = k$ and $j_{a,b,c} = 0$; and (b) $k_c = k$ and $j_{a,b,c} = 0.02$. To distinguish the edge and bulk modes, six chosen frequencies are highlighted in different colors in band structure diagrams (left panels) and corresponding mode shape diagrams (right panels). The middle panels show the magnified frequency range of the first bandgap with residing three interface modes.

phase of each isolated band below that gap according to Eq. (9), are determined in two different unit cell configurations $k_1 > k_2$ and $k_1 < k_2$. One can observe a strong influence of the stiffness of TNN coupling springs on dispersion curves. Figure 2(a) shows the case of the strongest TNN coupling when $k_1 = k_2$ (left panel) and $k_1 \lesseqgtr k_2$ (right panel). The case of equal springs in NN interactions shows two Dirac points, with a single gap (highlighted in gray color) between the second and third bands. The case of different NN coupling springs leads to the emergence of band-folding induced bandgaps, which yields the same band structure but different topological properties of isolated bands in two configurations i.e., $\theta^{\text{Zak}}_{(m)} = 0$ for all bands when $k_1 < k_2$ and $\theta^{\text{Zak}}_{(m)} = \pi$ for $k_1 > k_2$ for all bands. This gives different signs of gaps in the first and third gaps (highlighted in purple color) indicating their non-trivial nature, while the second gap is trivial due to the same signs. It should be emphasized that the non-trivial gaps are very narrow in the strong stiffness TNN coupling. A decrease of the TNN interaction stiffness k_c leads to the widening of non-trivial gaps, which are the largest for the lowest BNN coupling stiffness [Fig. 2(d)]. The effect of introduced inerter devices used in both NN and BNN couplings is reflected in decreased frequencies of dispersion branches, especially in the higher frequency bands. However, no changes

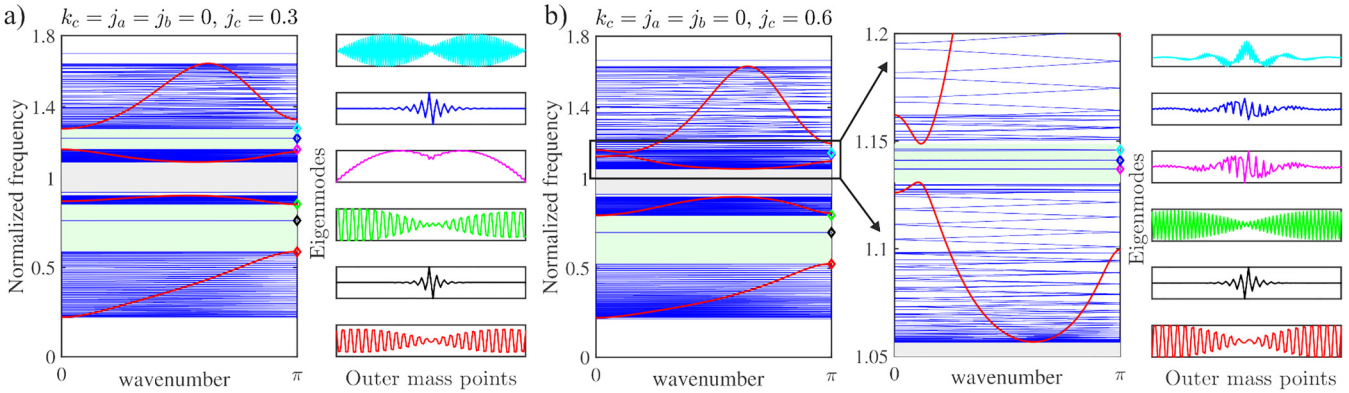

FIG. 5. Band structure and eigenmode diagrams of a supercell with 40 unit cells on each side of the interface (overall 324 masses) without TNN springs and with strong TNN inerter-based interactions. The case of $\gamma = 0.5$ ($k_1 > k_2$) is adopted in two different configurations: (a) $k_c = j_{a,b} = 0$ and $j_c = 0.3$; and (b) $k_c = j_{a,b} = 0$ and $j_c = 0.6$. To distinguish the edge and bulk modes six chosen frequencies are highlighted in different colors in band structure diagrams (left panels) and corresponding mode shape diagrams (right panels). The middle panel in sub-figure (b) shows the magnified frequency range of the third bandgap with residing three interface modes having mode shapes with weak localization properties.

occur in the topological properties of the system (e.g., see Ref. 31) and all the bands have the same topological invariants when weak NN and TNN inerters are used.

B. Spatial and frequency localization

Figure 3 is the parametric study showing the influence of nonlocal spring and inerter coupling on the band structure and mode shapes of a supercell system with 324 masses (including local resonator masses), which demonstrates the existence of interface states and enables us to count their overall number. It can be noticed that excellent matching of the bulk bands with the dispersion branches (full red lines) was obtained from the corresponding simple unit cell model. Figure 3(a) refers to the configuration without TNN coupling $k_c = 0$ and inerter elements in the system. One can observe two interface modes in the band diagram, one in each of the two non-trivial gaps (gaps highlighted in green color), whose mode shapes, given in panels on the right-hand side, demonstrate the spatial localization of those modes at the interface. These mode shapes (blue and black lines) can be considered symmetric, where the interface mass is at rest while the neighboring masses have equal amplitudes but opposite phases. The mode shapes from the bulk frequencies display the typical features of the conducting modes while a single interface mode (colored in green) from the trivial bandgap is also localized but displays anti-symmetric properties, i.e., interface and neighboring masses are displaced from the equilibrium point. Similar mode shapes occur in the configuration with considered inerter elements both in the NN and TNN coupling when $j_a = j_b = j_c = 0.02$ given in Fig. 3(b). Note that in all observed super-cell configurations, we adopted the NN coupling stiffness parameter to be $\gamma = 0.5$ (i.e., $k_1 > k_2$), resulting in stronger stiffness of interface springs and leading to the symmetric mode shapes mentioned earlier, with constant frequency for varying positive values of γ (e.g., see Ref. 31). Conversely, taking negative γ, related to $k_1 < k_2$, will yield weaker stiffness of interface springs, resulting in anti-symmetric lattice mode shapes whose frequency varies for different negative values of γ. The physics behind the formation of these symmetric and anti-symmetric mode shapes was explained in Ref. 32 for simple phononic lattices. However, the analysis of this phenomenon becomes more complex for lattices with multiple interface modes within a single gap and will be omitted in this work. Further, under the influence of inertance, one can observe a significant shifting of both bulk band and interface mode frequencies to lower values of frequencies can be observed while maintaining the same number of interface states. This demonstrates the potential of mechanical inerters to control the band structure properties of lattices and especially the interface states. The effect of stiffness of TNN spring k_c is investigated in Figs. 3(c), 3(d) and 4. Low values of $k_c = 1/10k$ demonstrated a weak influence on both band structure and mode shapes compared to the configuration without them, i.e., the overall number of interface modes and their mode shapes remain the same. Further increase of $k_c = 1/3k$ leads to significant changes in band frequencies and mode shapes. Moreover, two new interface modes within the non-trivial gaps emerged from the bulk, whose mode shapes (see red and magenta mode shapes) are localized around the interface in the form of anti-symmetric modes while the standard simple unit cell model yields the winding number difference $w = 1$. The other two interface modes inside the non-trivial gaps remain in a similar symmetric mode shape form. Finally, Fig. 4 shows the effect of strong stiffness TNN coupling $k_c = k$ with the main consequence of an increased number of interface modes. Three interfaces exist in each of the two non-trivial bandgaps whose localization is demonstrated through eigenmode analysis. All three modes display different shapes in the form of symmetric or anti-symmetric modes. However, due to nonlocal interactions, the zone of localization is widened, thus, significantly affecting the topological properties of the lattice which will be the subject of investigation in the following subsection.

Figure 5 shows the effect of increased inertance in inerter-based TNN interactions on the super-cell band structure and mode

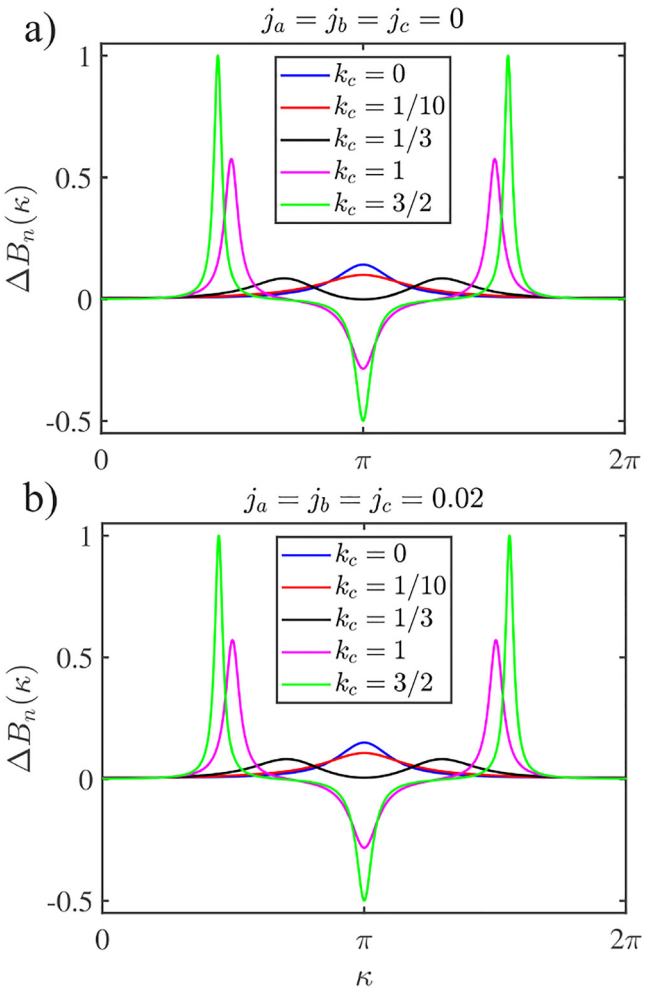

FIG. 6. The difference in Berry connection curves $\Delta B(\kappa)$ of two unit-cell configurations $\gamma = \pm 0.5$ given for $\kappa = 0 - 2\pi$ (a) without inerters; and (b) with weak inerter-based NN and TNN interactions. Curves in each panel refer to different stiffnesses of TNN spring k_c showing peaks and valleys of the first band.

shapes. The results clearly show that higher values of inertance, along with the lack of TNN spings and NN inerters $k_c = j_a = j_b = 0$, can affect the topology of the higher frequency bandgap by significantly reducing its width while leading to the emergence of three interface modes. In the configuration with $j_c = 0.3$ the influence of TNN inerter is visible but the number of interface states remains the same as in the configuration without it. On the other side, the stronger inertance $j_c = 0.6$ leads to almost overlapping of the bulk modes narrowing the bandgap in between, which have three interface modes residing inside it. Their localization properties are demonstrated through eigenmode analysis that reveals that the first bandgap interface mode is still localized in the form of symmetric mode. However, the narrow bandgap interface modes barely exist, and their localization is highly affected showing significant disturbances far from the interface. These results bring us to the conclusion that one needs to be careful with the choice of inerter parameters in TNN coupling since it leads to the partial delocalization of the interface modes.

C. Berry connection and winding number

In the preceding analysis, we demonstrated the non-trivial topology of certain bandgaps in the system and explored the existence of interface modes within those gaps through the band analysis of the super-cell. We have shown that the topological invariant Zak phase can be utilized in determining the sign of the gap i.e., the band transition between two lattices with alternating stiffness, which will tell us whether the corresponding gap is non-trivial or the trivial one but cannot give us information of the number of interface states. The winding number is another topological invariant that can be used in evaluating the topological properties of the lattice along with determining the number of interface/edge states. Such gauge-dependent invariant is also related to the Zak phase and measures the rotation of eigenvectors around the center of the complex plain. In Ref. 23 the authors have shown that an alternative formula for the winding number of the SSH chain with BNN interaction yields the same values of this invariant that is equal to the winding number difference of one, which on the other side fails to predict the correct number of interface states. For this purpose, the correct number of states was predicted by calculating the number of peaks and valleys on the Berry connection curve or through the Jackiw–Rebbi zero modes. Another important issue is the calculation of winding numbers and non-trivial topology in multiband systems, where each dispersion band can exhibit a unique value of the winding number. In Ref. 6 it was proposed to introduce a unique winding number for each of the gaps we want to evaluate, which is obtained by summing the winding numbers of all bands below that gap. It was discovered that the emergence of edge modes is related to odd values of this unique number. In this work, the winding number calculation can be done based on the Zak phase which then predicts the same winding number $w = 1$ for all of the bands of locally resonant lattice without and with weak TNN couplings ($k_c = 1/10k$). However, stronger spring TNN coupling ($k_c = 1/3k$ and $k_c = k$) results in a higher number of interface modes while the winding number is the same. Therefore, to follow these changes solely based on the simple unit cell band structure and since the number of topologically protected states depends on the topological invariant difference due to differences in gauges,[23] we suggest plotting the difference of a Berry connection curve in two configurations when $\gamma = \pm 0.5$.

Figure 6 shows five distinct Berry connection difference curves, each referring to different stiffness of TNN springs in the case with and without TNN inerter-based interactions. Note that in this figure only $\Delta B(\kappa)$ for the first band is given since the results for the other three bands are similar in shape. Obtained curves $\Delta B(\kappa)$, without and with weak stiffness TNN coupling yield a single peak that corresponds to the winding number $w = 1$. However, higher values of stiffness of TNN springs lead to the emergence of two peaks and one valley, which corresponds to higher values of interface states that cannot be predicted by the conventional winding number methodology. The major transition

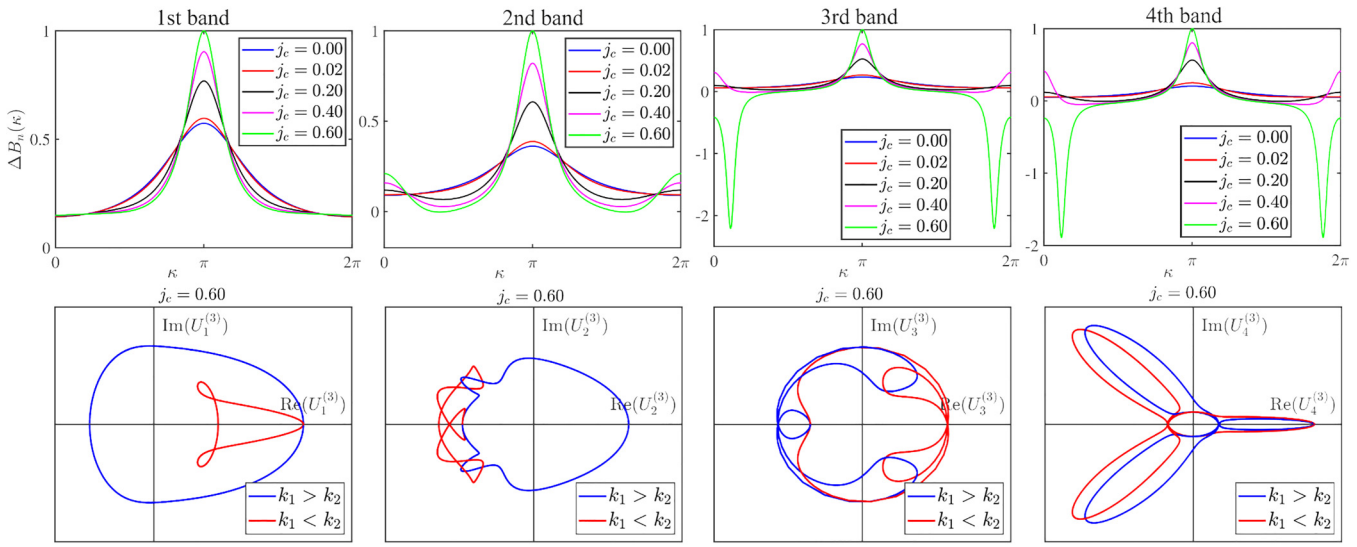

FIG. 7. The difference in Berry connection curves, $\Delta B(\kappa)$ (first-row panels), and the variation of the corresponding complex eigenvector component (second-row panels) as a function of the wavenumber κ for all four bands in two unit-cell configurations, $k_1 \lessgtr k_2$, is presented for the case when $k_c = j_a = j_b = 0$. The Berry connection curves in each panel from the first row refer to different inerter-based TNN interactions, j_c, showing peaks and valleys. The top view (hiding the third momentum space dimension) of the rotation of eigenvectors of the corresponding bands around the center of the complex plane can be observed for $k_1 > k_2$ (blue lines in the lower panels), referring to the winding number of $w = 1$, while the case without rotation, $k_1 < k_2$ (red lines in the lower panels), corresponds to $w = 0$. Note that only a single of two complex eigenvector components is plotted, as they behave in the same way for the observed lattice configurations.

point between single and multiple peaks and valleys is related to the BNN stiffness $k_c = 1/3k$, which is in line with the results achieved in a two-band system referring to the simple SSH chain presented in Ref. 23. Despite this unique number of peaks and valleys in each band can give us information about certain changes in the lattice, and it also matches the number of interface states in non-trivial gaps, no generic rule can be defined in a multi-band system to calculate the number of TPIS.

The previous analysis is especially interesting in the following case where only a strong TNN inerter-based coupling is presented (see Fig. 7), where $\Delta B(\kappa)$ along with the visualization of complex eigenvector components is given for all four bands. The obtained results demonstrate a significant influence of TNN inerters on the topological properties of higher frequency bands. More precisely, a difference in Berry connection curves becomes obvious for the last two bands (bands III and IV), where the higher values of inertance lead to the emergence of two valley-like peaks, thus indicating changes in the gauge. As given in Ref. 23, the positive signs of local peaks in $\Delta B(\kappa)$ diagrams correspond to higher winding numbers which again match with the number of TPIS from the super-cell analysis. Opposite to this, when there is a flip of peaks and valleys, the winding number prediction fails to match the number of TPIS and the winding number difference of one occurs. A similar situation is happening in our case, where the winding number difference of one occurs in all four bands, as visualized from the complex components of the eigenvectors (the panels in the second row of Fig. 7) when $j_c = 0.6$, also corresponding to the case with two valleys and one peak in the third and fourth modes. Note that even though both the third and fourth components of the eigenvectors are complex, for the sake of clarity only the third one is plotted since the other one behaves in the same way and the surface between these two component lines also encloses the complex origin indicating the winding number $w = 1$. It should also be emphasized that the winding number $w = 1$ is related to the first and second bands in the configuration $k_1 > k_2$, and to the third and fourth bands in the case of $k_1 < k_2$, and vice versa for $w = 0$, as can be seen from the second-row panels of Fig. 7. These changes are also confirmed in the supercell band structure analysis and the corresponding mode shapes, where three interface-like modes emerged within the third narrow frequency bandgap.

The preceding theoretical analysis demonstrated the remarkable control potential of ideal inerter devices in manipulating band structure and topological properties of lattices with NN and BNN interactions. Though the achieved results are promising from the viewpoint of introduced novel passive components to control wave propagation in periodic systems, it is an open question what values of inertance parameter can be realistically achieved in mechanical inerters having in mind its significant influence. Some designs of mechanical inerters were suggested in Ref. 31 but this subject is still open for further research both experimentally and theoretically.

V. CONCLUSION

This theoretical study delves into the fascinating realm of topological interface states emerging within the one-dimensional inerter-based locally resonant lattices featuring beyond-nearest neighbor coupling. By introducing third-nearest neighbor interactions, the lattice system unveils nontrivial topological behavior,

giving rise to robust and protected interface states within the lattice bandgap. These states exhibit distinctive spatial and frequency localization properties, presenting compelling opportunities for efficient signal manipulation and control. The observed topological phase transitions, as a consequence of broken inversion symmetry that lifts the degeneracy and opens non-trivial bandgaps, further amplify the lattice system's versatility. The presence of inerters in the third-nearest neighbor interactions significantly impacts both the band structure and the topological properties of the lattice. Consequently, incorporating inerters in the locally resonant lattices with beyond-nearest neighbor coupling bears substantial implications for advanced device and system design. These findings lay a robust foundation for the development of topological waveguides, filters, and sensors with heightened robustness and performance. Key novelties of this paper include:

- *Incorporation of Third-Nearest Neighbor Interactions*: This study uniquely explores the impact of third-nearest neighbor interactions in inerter-based locally resonant lattices, revealing the maintained non-trivial topological behavior for weak inertance values.
- *The emergence of Robust Interface States*: The research identifies and characterizes topologically protected interface states within the lattice bandgap, showcasing their unique spatial and frequency localization properties.
- *Versatility through Inerter-based Design*: The incorporation of inerters enhances the lattice system's versatility, allowing for the significant manipulation of topological properties not only through variations of stiffness and mass properties but also the inertance in both nearest-neighbor and beyond-nearest neighbor interactions.
- *Significant Influence on Band Structure and Topological Properties*: The unique band structure of the locally resonant lattice, presence of topological interface states and phase transitions induced by the broken inversion symmetry through alternating stiffness of springs in the nearest-neighbor coupling can be controlled through inerter devices, which significantly influences both the frequencies of the band structure and the topological interface states.
- *Implications for Advanced Device Design*: The incorporation of inerters in locally resonant lattices with beyond-nearest neighbor coupling holds promise for the design and implementation of passive or semi-passive control in advanced devices, such as topological waveguides, filters, and sensors.

Future works originating from this paper could include the practical development of novel devices for control and manipulation of propagating waves within the lattice system, exploration of higher-dimensional lattices and longer nonlocal hoppings, and alternative damping schemes to expand the range of topological effects and their applications. This research deepens our understanding of topological phenomena in complex lattice structures and paves the way for future studies and innovations in the realm of topological metamaterials.

ACKNOWLEDGMENTS

M.C. and D.K. wish to acknowledge support of the Ministry of Science, Technological Development, and Innovation of the Republic of Serbia for their support through the Mathematical Institute of the Serbian Academy of Science and Arts.

AUTHOR DECLARATIONS

Conflict of Interest

The authors have no conflicts to disclose.

Author Contributions

Milan Cajić: Conceptualization (equal); Methodology (lead); Software (lead); Validation (lead); Visualization (lead); Writing – original draft (lead). **Danilo Karličić:** Writing – original draft (supporting); Writing – review & editing (equal). **Sondipon Adhikari:** Conceptualization (equal); Writing – original draft (supporting); Writing – review & editing (equal).

DATA AVAILABILITY

The data that support the findings of this study are available from the corresponding author upon reasonable request.

REFERENCES

[1]Z. Zheng, J. Yin, J. Wen, and D. Yu, "Higher-order topological states in locally resonant elastic metamaterials," Appl. Phys. Lett. **120**, 144101 (2022).
[2]W.-Y. Zhang, H. Chen, H.-S. Lai, J.-L. Xie, C. He, and Y.-F. Chen, "Multimode topological interface states in a one-dimensional elastic-wave phononic crystal," Phys. Lett. A **479**, 128929 (2023).
[3]M. Xiao, G. Ma, Z. Yang, P. Sheng, Z. Zhang, and C. T. Chan, "Geometric phase and band inversion in periodic acoustic systems," Nat. Phys. **11**, 240 (2015).
[4]G. Ma, M. Xiao, and C. T. Chan, "Topological phases in acoustic and mechanical systems," Nat. Rev. Phys. **1**, 281 (2019).
[5]H.-T. Chen, C.-H. Chang, and H.-C. Kao, "Connection between the winding number and the Chern number," Chin. J. Phys. **72**, 50 (2021).
[6]H. Al Ba'ba'a, M. Nouh, and T. Singh, "Dispersion and topological characteristics of permutative polyatomic phononic crystals," Proc. R. Soc. A **475**, 20190022 (2019).
[7]C.-S. Lee, I.-F. Io, and H.-C. Kao, "Winding number and Zak phase in multi-band SSH models," Chin. J. Phys. **78**, 96 (2022).
[8]J.-Y. Kuo, T.-Y. Lee, Y.-C. Chiu, S.-R. Liao, and H.-C. Kao, "SSH coupled-spring systems," arXiv:2310.00547 (2023).
[9]A. Marques and R. Dias, "One-dimensional topological insulators with noncentered inversion symmetry axis," Phys. Rev. B **100**, 041104 (2019).
[10]G.-Q. Li, B.-H. Wang, J.-Y. Tang, P. Peng, and L.-W. Dong, "Topological properties of tetratomic Su–Schrieffer–Heeger chain with hierarchical long-range hoppings," Chin. Phys. B **32**, 077102 (2023).
[11]A. Marques and R. Dias, "Generalization of Zak's phase for lattice models with non-centered inversion symmetry axis," arXiv:1707.06162 (2017).
[12]J.-W. Rhim, J. Behrends, and J. H. Bardarson, "Bulk-boundary correspondence from the intercellular Zak phase," Phys. Rev. B **95**, 035421 (2017).
[13]R. Leone, "The geometry of (non)-Abelian adiabatic pumping," J. Phys. A: Math. Theor. **44**, 295301 (2011).
[14]F. Farzbod and O. E. Scott-Emuakpor, "Interactions beyond nearest neighbors in a periodic structure: Force analysis," Int. J. Solids Struct. **199**, 203 (2020).
[15]R. Fleury, "Non-local oddities," Nat. Phys. **17**, 766 (2021).

[16]Y. Chen, M. Kadic, and M. Wegener, "Roton-like acoustical dispersion relations in 3D metamaterials," Nat. Commun. **12**, 3278 (2021).
[17]L. Iorio, J. M. De Ponti, F. Maspero, and R. Ardito, "Roton-like dispersion via polarisation change for elastic wave energy control in graded delay-lines," J. Sound Vib. **572**, 118167 (2024).
[18]W. Y. Yang, Y. Zhuang, L. A. Darcy, G. Liu, and A. Ion, "Reconfigurable elastic metamaterials," in *Proceedings of the 35th Annual ACM Symposium on User Interface Software and Technology* (Association for Computing Machinery, 2022), pp. 1–13.
[19]Y. Chen, K. Wang, M. Kadic, S. Guenneau, C. Wang, and M. Wegener, "Phonon transmission through a nonlocal metamaterial slab," Commun. Phys. **6**, 75 (2023).
[20]R. Dias and A. Marques, "Long-range hopping and indexing assumption in one-dimensional topological insulators," Phys. Rev. B **105**, 035102 (2022).
[21]H. Chen, H. Nassar, and G. Huang, "A study of topological effects in 1D and 2D mechanical lattices," J. Mech. Phys. Solids **117**, 22 (2018).
[22]H. Liu, X. Huang, M. Yan, J. Lu, W. Deng, and Z. Liu, "Acoustic topological metamaterials of large winding number," Phys. Rev. Appl. **19**, 054028 (2023).
[23]A. Rajabpoor Alisepahi, S. Sarkar, K. Sun, and J. Ma, "Breakdown of conventional winding number calculation in one-dimensional lattices with interactions beyond nearest neighbors," Commun. Phys. **6**, 334 (2023).
[24]Y. Liu, H. Wang, W. Fang, Q. Han, D. Liu, and Y. Liang, "Tunable control of subwavelength topological interface modes in locally resonance piezoelectric metamaterials," Compos. Struct. **276**, 114541 (2021).
[25]Z. Wu, R. Xia, J. Yi, and Z. Li, "Multiple topological interface modes in electromechanically resonant piezoelectric beams," Eng. Struct. **281**, 115716 (2023).
[26]P. Li, W. Hu, P. Peng, X. Zhu, and D. Zhao, "Elastic topological interface states induced by incident angle," Int. J. Mech. Sci. **225**, 107359 (2022).
[27]J. W. You, Z. Lan, Q. Ma, Z. Gao, Y. Yang, F. Gao, M. Xiao, and T. J. Cui, "Topological metasurface: From passive toward active and beyond," Photonics Res. **11**, B65 (2023).
[28]H. Al Ba'ba'a, X. Zhu, and Q. Wang, "Enabling novel dispersion and topological characteristics in mechanical lattices via stable negative inertial coupling," Proc. R. Soc. A **477**, 20200820 (2021).
[29]C. Papageorgiou, N. E. Houghton, and M. C. Smith, "Experimental testing and analysis of inerter devices," J. Dyn. Syst. Meas. Control **131**, 011001 (2008).
[30]C. Liu, L. Chen, H. P. Lee, Y. Yang, and X. Zhang, "A review of the inerter and inerter-based vibration isolation: Theory, devices, and applications," J. Franklin Inst. **359**, 7677 (2022).
[31]M. Cajić, D. Karličić, J. Christensen, and S. Adhikari, "Tunable topological interface states in one-dimensional inerter-based locally resonant lattices with damping," J. Sound Vib. **542**, 117326 (2023).
[32]R. K. Pal, J. Vila, M. Leamy, and M. Ruzzene, "Amplitude-dependent topological edge states in nonlinear phononic lattices," Phys. Rev. E **97**, 032209 (2018).